16th World Conference on Earthquake, 16WCEE 2017

Santiago Chile, January 9th to 13th 2017

Paper N° 666

Registration Code: S-X1461296258

Seismic Retrofitting Effects of Steel Brace on Capacity of Shear-Critical RC Frame Using Round Bars

K. Tajima[1], R. Satoh[2], S. Uchino[3], K. Naganuma[4], N. Shirai[5]

[1] *Associate Professor, Nihon University, tajima.kazuki@nihon-u.ac.jp*
[2] *Master of Eng., Kume Sekkei, Ryosuke.Sato@kumesekkei.co.jp*
[3] *Master of Eng., Kawada Industries, suguru.uchino@kawada.co.jp*
[4] *Professor, Nihon University, naganuma.kazuhiro@nihon-u.ac.jp*
[5] *Professor, Nihon University, shirai@arch.cst.nihon-u.ac.jp*

Abstract

After the Hyogo-KEN Nanbu Earthquake, existing R/C buildings in Japan, violating the current criteria of design code, have been seismically retrofitted with various reinforcing components. In most cases, among the available retrofitting systems, the steel bracing system was preferably adopted, because the weight of this system is lighter than the other systems and it can provide moderate openings. However, in order to assess the effect of seismic retrofitting by steel bracing system correctly, there are still remained three issues to be solved as follows:

1) Up to now, the reinforcing effect of steel bracing has been mostly investigated through the test on R/C sub-frame specimens with single story and span. Thus, the impact of single and/or multiple steel bracing systems incorporated in R/C framed structures on the overall capacity of building with multiple stories and spans is not clarified.

2) Some critical aspects involved in the existing R/C buildings designed according to the old seismic design code in Japan are the shear failure of columns and the bond-slip behavior of round longitudinal bars in columns. The influence of these behaviors on the capacity of R/C structures is not fully understood.

3) Effect of the structural slits, usually made for the non-structural walls during the retrofit work, on the seismic retrofitting performance has not been clearly investigated.

The short columns with non-structural walls tend to cause brittle shear failure. Thus, it is recommended to make structural slits such that the height of column becomes longer and leads to ductile flexural failure. However, the effect of the structural slits is not clearly verified. Three single-story and two-span R/C framed specimens were made; the first one is the reference specimen with non-structural walls, designed according to the old seismic code, and the other two are the retrofitted specimens by the steel bracing unit and/or the structural slits, and the static cyclic loading tests were performed. The test results demonstrated that the superior retrofitting effect of the steel bracing system, enhancing the capacity of R/C framed specimen, could be evaluated quantitatively.

Furthermore, the test results indicated that the structural slits were effective for preventing the shear failure of column. On the other hand, it could be pointed out that the structural slits might not improve deformability of the retrofitted framed specimens. The source of insufficient deformability may be partly due to severe fractures at the indirect joints of mortar between the R/C frame and the steel frame along the columns. It seems that this joint fracture might be due to the stiffness degradation caused in column by introducing the structural slits. Also, the bond-slip of longitudinal round bars in the columns might contribute to the additional stiffness reduction of the columns.

Finally, in order to investigate the development of stress resultants such as shearing and axial force in columns and steel braces and the seismic resisting mechanism of the steel brace-frame system, the nonlinear finite element analyses were carried out.

Keywords: Reinforced Concrete; Seismic Retrofit; Steel Brace; Shear Failure; Nonlinear FE Analysis

1. Introduction

Among various seismic retrofitting techniques developed in Japan, the steel bracing system has been frequently applied to the existing R/C buildings, because it has lighter weight and makes possible provide moderate openings. This system came into wide use after the Hyogo-ken Nanbu earthquake in 1995. This system experienced the Great East Japan Earthquake in 2011, but the subsequent damage investigation verified its effectiveness. However, there are still remained several issues to be solved to evaluate the effect of seismic retrofitting by the steel bracing unit in a rational way. It must be noted that the retrofitting effect of the system has been mainly investigated on the basis of test results on single-story and -span framed specimens due to the experimental limitation. For this reason, the impact of single and/or multiple steel bracing units installed in the R/C frames on the overall capacity of building with multiple stories and spans has not been clearly understood.

Columns in the R/C buildings constructed before 1970 tend to fail in shear, because they were mostly made of low-strength concrete and reinforced with small amount of hoops. In addition, the round bars were utilized as the longitudinal bars in those days, but the influence of bond slip behavior between concrete and steel bar on the retrofitting effect had not been sufficiently investigated. Furthermore, many existing R/C school buildings retrofitted with the steel bracing unit have monolithically placed non-structural walls such as the hanging wall and the spandrel wall with columns, and consequently these columns become the short column leading to a brittle shear failure. In case of retrofitting, it is desirable to make the structural slits between non-structural walls and columns for avoiding the shear failure in columns. However the retrofitting effect of structural slits has not been sufficiently clarified.

This paper focuses on sub-frames at the first story in the existing R/C school buildings erected in the 1960s. Alternative lateral cyclic loading tests on single story and two span R/C sub-frame specimens are conducted and test results are presented. Three specimens were tested; the first one is a reference sub-frame with the hanging and spandrel walls but without the structural slits and the steel bracing unit, the second one is a sub-frame with the steel bracing unit but without the structural slits, and the third one is a sub-frame with the steel bracing unit as well as the structural slits. Furthermore, variation in the shear failure mode of columns caused by the retrofitting and also variation in the resistant mechanism of the steel bracing unit with fracture development along the indirect mortar joints between the steel frame and the main R/C frame shall be discussed. It is usually difficult to evaluate variation in axial and shearing forces in the columns with development of shear fracture experimentally. In this study, the redistribution of axial and shearing forces in the columns shall be investigated using a nonlinear finite element analysis.

2. Cyclic Loading Test on R/C Framed Specimens with Steel Brace

2.1 Outline of specimens

One-third scaled single story and two span frame specimens were designed with reference to the existing R/C school buildings erected in 1960s. The configuration and detail of specimens are shown in Fig.1. The design parameters of specimens are whether the steel bracing unit and the structural slits in the non-structural walls facing to the columns are present or not. Three specimens were prepared; RCW with the hanging and spandrel walls and without bracing unit, RCWB with the hanging and spandrel walls and the bracing unit, and RCB with bracing unit and without the hanging and spandrel walls. The columns in RCW become highly brittle failure type due to the existence of the hanging and spandrel walls. RCWB was made from RCW by removing the hanging and spandrel walls in the span in one side and filling the steel bracing unit with the indirect joint. Note that RCB is the specimen removing the non-structural walls from RCWB, to neglect the effect of the hanging and spandrel walls with the slits having the width of about 100 mm in the both side on behavior of the adjacent columns.

The mechanical properties of concrete and steel bars are listed in Table 1. The specified strength of concrete was F_c = 18 N/mm^2. SR235 was used as the rebars; 12-9φ, p_g = 1.9 %. The round bars with small diameter were used as the hoops; f_y = 291 N/mm^2, 2-4.4φ, p_w = 0.095 %. The thickness of non-structural walls is 60 mm, and the round bars with diameter of 9 mm were distributed at the interval of 100 mm in the vertical and horizontal direction. The steel brace member of SS400 with the section of BH-50 x 50 x 45 x 45 was used. The frame component of bracing unit has the same H-shaped section as the brace component, and is able to resist the unbalance force induced in the brace components. The anchors and the headed studs were arranged in the interval of 80 mm, and the spiral reinforcement was inserted inside the retrofit joints in the interval of 30 mm. The specified strength of mortar filling up the retrofit joint was F_c = 30 N/mm^2. Note that the measured yield strengths of rebar in the column and steel brace highly exceeded the specified values.

The calculated values of design strength for the columns are listed in Table 2. The ultimate flexural moment M_u (kNm), the shearing force at the ultimate flexural moment Q_{mu} (kN) and the ultimate shear strength Q_{su} (kN) were calculated according to the following equations:

$$M_u = 0.8 a_t \sigma_y D + 0.5ND\left(1 - \frac{N}{bDF_c}\right) \tag{1}$$

$$Q_{mu} = \frac{2M_u}{h_0} \tag{2}$$

$$Q_{su} = \left\{\frac{0.053 {p_t}^{0.23}(F_c+18)}{M/_{Qd}+0.12} + 0.85\sqrt{p_w \sigma_{wy}}\right\} bj + 0.1\sigma_0 bj \tag{3}$$

where, a_t : the area of tensile reinforcing bars (mm^2), σ_y : the yield strength of rebar (N/mm^2), D : the depth of column (mm), N : the axial force (kN), b : the width of column (mm), F_c : the specified strength of concrete (N/mm^2), h_0 : the clear height of column (mm), p_t : the steel ratio of tensile reinforcement, M/Qd : the shear-span ratio, p_w : the steel ratio of hoops, σ_{wy} : the yield strength of hoop (N/mm^2), j : the distance of lever arm (mm), σ_0 : the axial stress (N/mm^2). In this calculation, the axial force ratio of column (= $N/F_c bD$) was assumed to be 0.35 and thus N = 180 kN was used. The target ratio of Q_{mu} to Q_{su} was assumed to be from 0.6 to 0.7 so that the shear failure would precede the flexural failure.

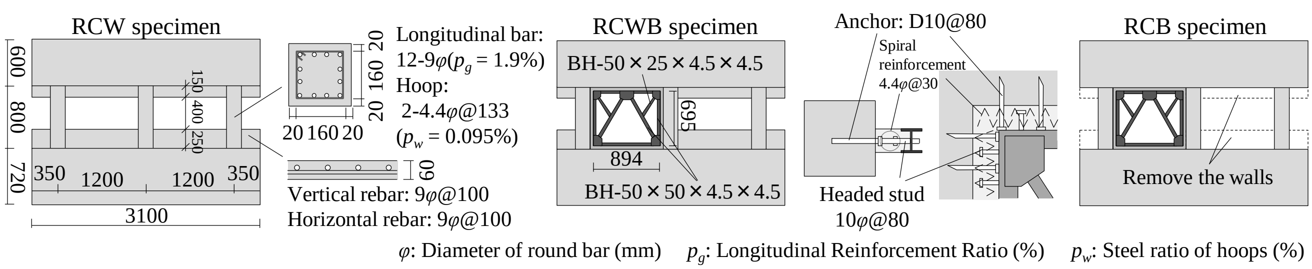

Fig. 1 – R/C framed specimens

Table 1 – Mechanical properties of concrete and steel

	Design value		Test result	
	F_c	E_c	σ_B	E_c
Concrete	18	20	21	24
Mortar	30	—	38	—

F_c: specified strength of concrete and mortar (N/mm^2)
E_c: Young's modulus of concrete (N/mm^2)
σ_B: concrete strength (N/mm^2)

	Design value		Test result	
	F or f_y	E_s	σ_y	E_s
Longitudinal bar	235	205	334	178
Hoop	291		268	184
Steel brace	245		334	182
Ancohr	295		353	177
Stud	295		343	171

F, f_y: specified yield strength of steel (N/mm^2)
E_s: Young's modulus of steel (N/mm^2)
σ_y: yield strength of steel (N/mm^2)

Table 2 – Design strength of columns

	Column with hanging wall and spandrel wall		Column without hanging wall and spandrel wall	
	Design strength using "Design value"	Design strength using "Test result"	Design strength using "Design value"	Design strength using "Test result"
Q_{mu} (kN)	115.3	139.6	57.7	69.3
Q_{su} (kN)	72.2	75.3	49.3	52.7
Q_{su} / Q_{mu}	0.63	0.54	0.86	0.76

2.2 Loading and measurements

The loading setup and the measuring devices of load and displacement are depicted in Fig.2. The lateral loading setup developed by the Building Research Institute in Japan was adopted. The installation position of lateral actuators was so determined on the basis of the reference specimen, RCW, that the lateral force would act at the mid-height of the clear column. The loading was carried out as follows. First, the axial force (540 kN) was applied to the specimen through the L-shaped loading beam, and then was controlled to keep a constant axial force. Next, the alternative cyclic lateral force was applied to the specimen by displacement control through the L-shaped loading beam. Applied forces were measured by the load cells attached to each actuator. Lateral and vertical displacements at the left and right lower corner of the top stub, as shown in Fig.2, were measured by using the displacement transducers mounted on the two steel posts settled on the bottom stab. The lateral displacement was controlled at the height of 1000 mm from the upper face of bottom stab. The reference control drift angle for the lateral loading shall be 1/1000. The drift increment shall be 1/1000 up to 5/10000, 2/1000 up to 12/1000 and 4/1000 up to 20/1000 by the displacement control. The number of alternative cycles shall be two up to the maximum strength, and thereafter it shall be one each.

Figure 3 shows the locations of strain gauges pasted on rebars and hoops, steel braces, anchors and headed studs. Five strain gauges (RCW, RCWB) and eight (RCB) were pasted on four longitudinal bars located at the corners in the column section. Four strain gauges were pasted on every single hoop. Four strain gauges were pasted on the side of each diagonal flange component in the steel bracing unit. The strain gauges were pasted on six anchors and on five studs in the retrofitted joints.

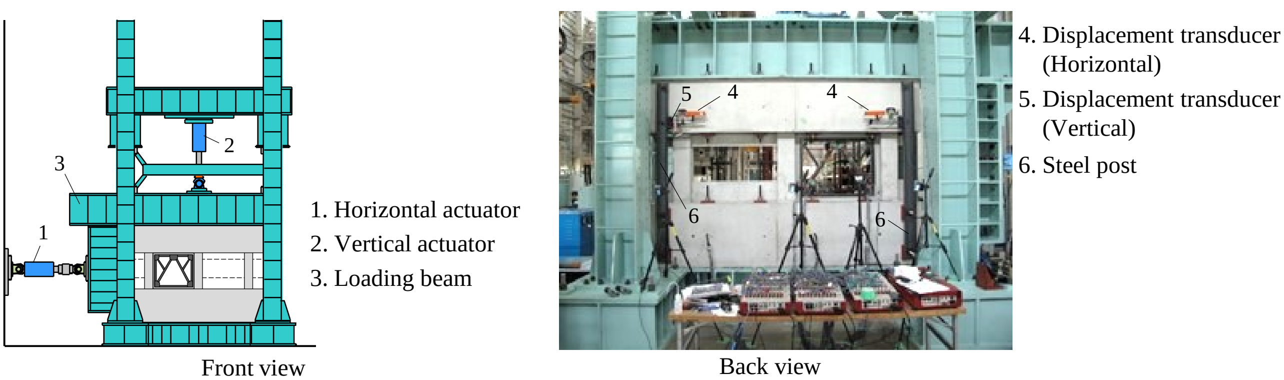

Fig. 2 – Loading setup and measuring devices of load and displacement

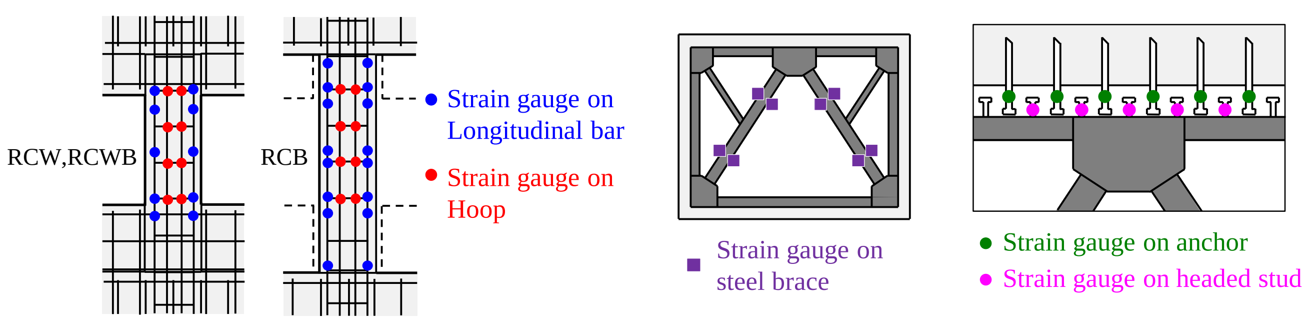

Fig. 3 – Locations of strain gauges

Figure 4 shows the image measurement procedure. Using the same procedure in the published paper [1], the image measurement on the column face was carried out by means of the digital camera to decompose deformation components along the column height. The aspect ratio of camera image is 3 versus 4. Since the width of column is 200 mm and the column deforms laterally under the loading condition, the width of acquisition image was set to be 270 mm. Thus, three cameras for each column, totally nine cameras were installed. The cameras with 12 million image pixels was utilized, and thus the size of single image pixel is about 0.009 mm. Before the measurement, the grid lines were drawn on the surface of specimen, and then the intersection point of grid lines shall be the target of measurement. Using the translational displacements at the target points, the flexural deformation component, δ_f , and the shear deformation component, δ_s , for the column can be calculated. Furthermore, the rotational deformation component, δ_r, caused by the pull-out of longitudinal round bars in the columns can be obtained by subtracting the sum of δ_f and δ_s from the total deformation, δ.

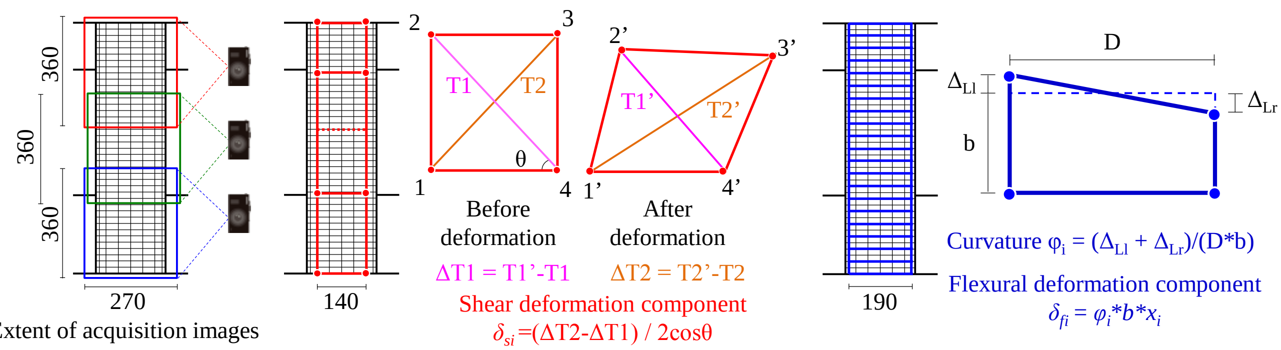

Fig.4 – Image measurement procedure

3. Test Results

3.1 Story shear force versus story drift angle relations

Figure 5 shows the story shear force (Q_{story}) - story drift angle (R) relations and the final failure pattern for each specimen.

It is seen from the comparison between the Q_{story} - R relations for RCW and RCWB that the maximum strength increases about 2.5 times by the retrofitting. Also, the drift angle at the maximum strength increases from 1/333 rad. to 1/166 rad., and thus the F-value, indicating the ductility index, improves from 0.8 to 1.2. In addition, the increase of initial stiffness can be clearly observed. As for the final failure pattern of RCW, all columns failed in shear in an early stage. In case of RCWB, on the other hand, the left column did not fail in shear and the drift angle of the remaining two columns at the shear failure increased.

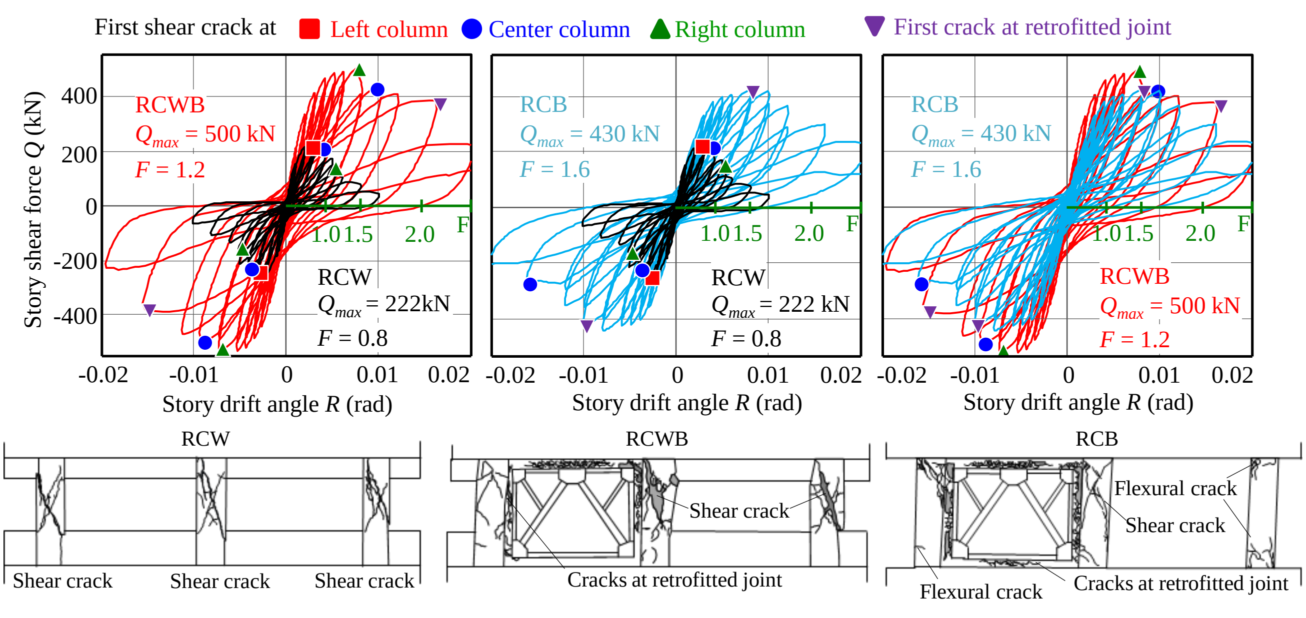

Fig.5 – Measured Q_{story} - R relations and observed final failure patterns

Next, it is seen from the comparison between the Q_{story} - R relations for RCW and RCB that the maximum strength increases about 2 times by the retrofitting. Also, the drift angle at the maximum strength increases from 1/333 rad. (F = 0.8) to 1/100 rad. (F = 1.6). Note that the increase of initial stiffness cannot be observed. This may be due to the stiffness degradation of each column by the structural slits. In case of RCB, the rotational deformation component dominates among the deformation component of columns, and as is seen from the fraction of shear deformation component to be described later, definite shear failure did not occur. Instead, the fracture concentrated on the retrofitted joints between the column and the bracing steel frame from an early stage. This might lead to the difference between the stiffness of R/C column and the steel bracing unit, and consequently induce the gap in their deformation patterns.

Finally, the Q_{story} - R relations for RCWB and RCB are compared. The maximum strength of RCWB is higher than RCB by about 10 percent and the stiffness is higher as well. On the other hand, the deformation of RCB at the maximum strength is larger than RCWB, and thus the F-value for RCB can be estimated to be higher by about 30 percent. Although the strength of RCWB reduced at the cycling of R = 1/166 rad., it retained the same strength as RCB at the cycling of R = 1/100 rad. Although RCWB was designed to raise the strength capacity, the fact that the deformation capacity increased could be explained by the bond-slip behavior of round bars as described earlier for RCW. After the peak capacity, the strength of RCWB gradually reduced up to the cycling of R = 1/63 rad. In case of RCB, on the other hand, the stress transfer mechanism between the R/C frame and the bracing steel frame was lost, and thus the strength reduction became rather significant than RCWB. As far as the specimens tested are concerned, it can be judged that the retrofitting effect of RCWB is higher than RCB. The source of this consequence must be attributed to the fracture in the retrofitted joints. Thus, it must be needed to take measures avoiding such fractures. Furthermore, the effect of stiffness reduction of columns must be investigated carefully when the structural slits are to be introduced.

3.2 Strain in hoops

Figure 6 shows the story drift angle, R, versus hoop strain, ε, relations and variation in the shear deformation components of the columns in the right side. The value of hoop strains in each column rapidly increased at the loading cycle when shear crack occurred, and reached to the yielding strain of 2000μ. Although three columns of RCW had the same section, the drift angles of each column, at which shear crack was first observed, were different from each other. This suggests that the effect of difference in the deformability of each column on overall behavior of the R/C structures needs to be investigated in detail.

In order to investigate the issue raised in the above, the shear deformation components of the right column in RCW, RCWB and RCB shall be compared. The right columns of RCW and RCWB failed in shear when the story drift reached 5 to 6 mm. The contributions of shear deformation of the right columns for all specimens are almost similar. The shear deformation of RCW and RCWB concentrated on the flexural height of columns (h_0 = 400 mm). In case of RCB, on the other hand, since the hanging and spandrel walls were removed, the flexural height of columns became h_0 = 800 mm, and thus the shear deformation spread over a wide portion of the column. Furthermore, the shear deformation angles of the right columns for RCW and RCWB were evaluated to be about 0.3 percent against 0.15 percent for RCB. These partly support the judgment that the failure did not occur in RCB. Thus, the retrofitting by the structural slit may be effective from a viewpoint that it prevents the shear failure of columns and the loss of column stability under axial forces.

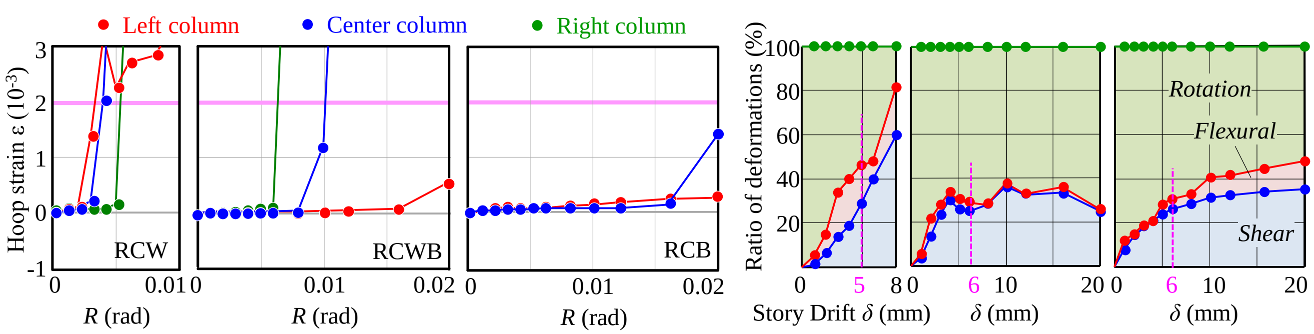

Fig.6 – Hoop strain ε - R relations and shear deformation components of right columns

3.3 Axial force and lateral force of steel braces

Figure 7 shows the internal axial force in the steel brace (N_B) versus the drift angle (R) relations and the resisting lateral force of bracing unit (Q_B) versus the drift angle (R) relations. RCWB, in which the retrofitted joints fractured, kept the axial force constant up to R = 1/63 rad. In case of RCB, on the other hand, the reduction of resisting axial force began at R = 1/125 rad., when severe cracks developed in the retrofitted joints, and especially the reduction of internal axial force in the resisting tensile brace was significant. Also, the reduction in resisting lateral force of brace unit began at R = 1/125 rad. Thus, it may be said that the fracture in the retrofitted joints exerted the ill effect on the retrofitting by the steel bracing system.

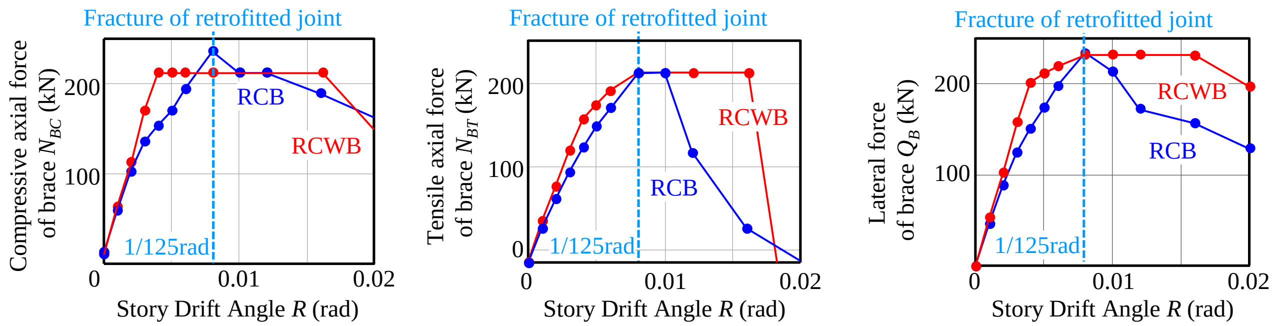

Fig.7 – N_B - R relations and Q_B - R relations

4. Nonlinear FE Analysis

The test results discussed in the previous sections suggest that the resisting mechanism of single-story and two-span R/C framed specimen changes with the development of fracture in a complex manner. However, it is difficult to clarify their resisting mechanisms experimentally due to the limited number of test specimens. In this study, nonlinear finite element (FE) analyses shall be conducted and discuss variation of the resisting mechanism of R/C frames. Especially, the FE analyses focus on the variation in the resisting lateral force and the axial force with the development of fracture in the column.

4.1 FE analysis for RCW specimen.

Figure 8 shows the mesh division for RCW. Two-dimensional analyses were carried out by utilizing the computer code called "FINAL" [2]. Concrete was expressed by the four-node plane stress element with about 25 mm each side, and the non-orthogonal smeared crack model was adopted. Rebars and hoops in the column were expressed by the truss element, and other steel bars were modeled by the embedded smeared reinforcement element. Since round bars were used as the longitudinal bars in the column, the bond-slip behavior along the height of column must be included in the analysis. For this purpose, the bond-slip behavior between concrete and steel bar was expressed by the inserted four-node interface element. Furthermore, to model the separation along the boundary between the columns and the non-structural walls, the discrete crack model was applied to the boundary.

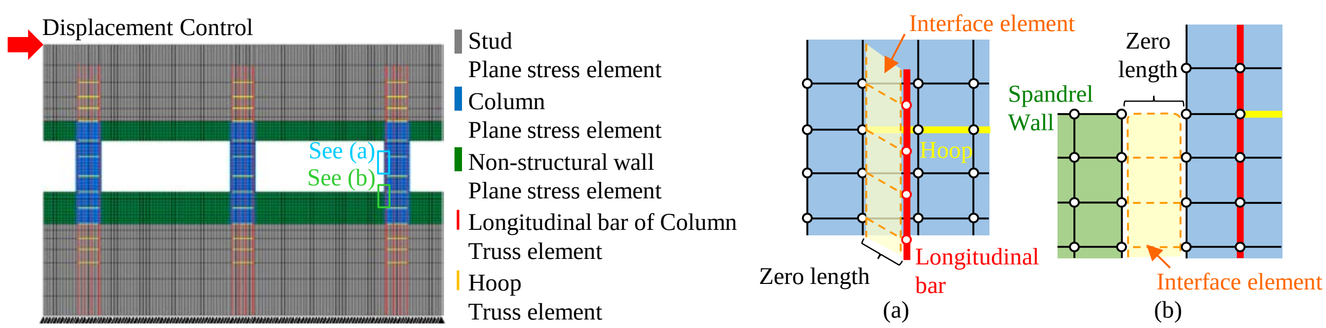

Fig.8 – Mesh division for RCW specimen

The stress (σ) versus strain (ε) relations for concrete and steel bars and the bond stress (τ) versus slip (S) relation are shown in Fig. 9. The post-peak σ - ε relation for concrete in the compression branch was expressed by the softening model including the compressive fracture energy G_{fc}, .The value of G_{fc} was calculated according to the formula presented by Nakamura et al. [3]. The characteristic length of element, l_{ch}, was assumed to be equal to the square root of element area, A. The ascending branch of tensile σ - ε relation for concrete up to the tensile strength, f_t, was assumed to be linear elastic, and the descending branch after the peak was expressed by the tension stiffening model presented by Naganuma et al. [4]. The hysteretic cyclic σ - ε relation of steel bars was expressed by the modified Menegotto-Pinto model presented by Ciampi et al. [5]. Note that the secondary slope was assumed to be 1/100 of the initial stiffness. The cyclic bond stress versus slip relation as well as the hysteresis loop for round bars was basically modeled by Naganuma, but the maximum bond stress and the subsequent softening branch were determined by the formulae by Matsuoka et al. [6]. The pullout displacement of wall reinforcement after cracking was included in the crack opening displacement of the discrete crack model [7]. The shear transfer behavior of concrete along cracks was expressed by the model presented by Naganuma [8].

Figure 10 shows the Q - R response as well as the cracking patterns at the maximum strength. The simulated hysteretic response including unloading and reloading is in good agreement with the test result. The predicted shear cracking in all columns at R = 3/100 rad. and the significant strength reduction occurred simultaneously. Although a time lag of shear cracking among the columns was not predicted by the analysis, the simulated failure pattern well corresponded to the test result.

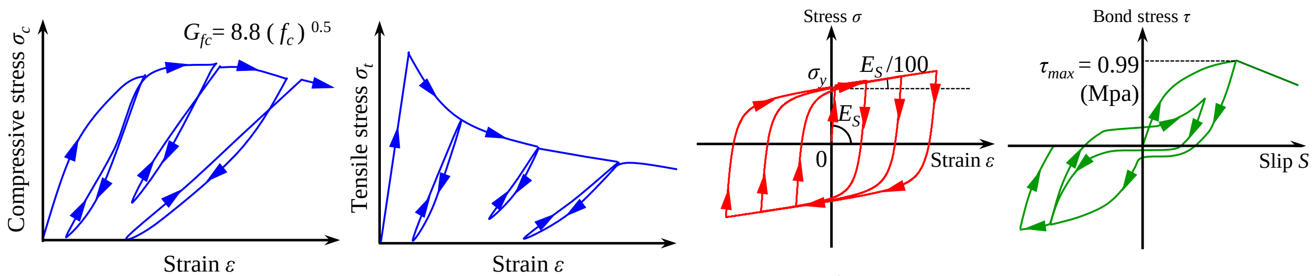

(a) Concrete (b) Reinforcing bar (c) Bond-slip relationship

Fig.9 – σ - ε relations of concrete and reinforcing bar and τ - S relation

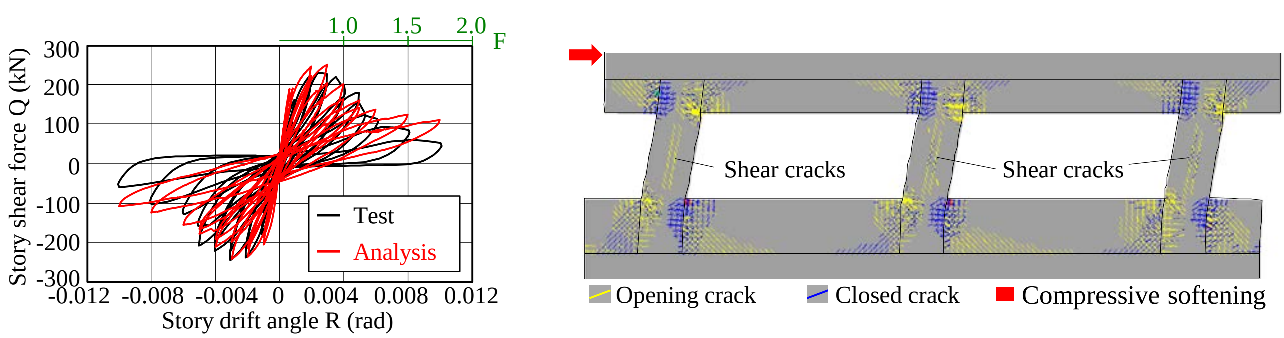

Fig.10 – Analysis results for RCW specimen

4.2 FE analyses for RCB and RCWB specimens

Figure 11 shows the mesh division of RCB. The modeling method and the constitutive law are similar to those of RCW in the previous section. For modeling the retrofitted joint, mortar was expressed by the four-node plane stress element, and studs and anchors were modeled as the smeared type embedded reinforcement. Furthermore, steel frame and braces were expressed by the beam element. In order to simulate the observed deterioration in lateral resistance of the bracing unit with the development of fracture along the retrofitted joints, the steel frame and mortar were separately discretized and the four-node interface element was inserted in between them. The normal stiffness under compression without opening displacement was assumed to be infinite. The pullout displacement of studs after cracking was included in the opening displacement under tension [9]. The shear stress versus slip displacement relation in the tangential direction was determined to be a tri-linear frictional type on the basis of the result on the pullout test of steel plate by Matsuura et al. [10]; where the frictional coefficient was assumed to be 0.4 in this study. For comparison and discussion, the analysis without the interface element was also carried out.

Figure 12 shows the Q - R response obtained by the analysis model with the inserted interface element between the steel frame and mortar, the variation of resisting lateral forces of the bracing unit under the positive loading, and the cracking pattern at the maximum strength. Note that only the predicted values up to R = 12/1000 rad., where solution became unstable, were plotted in the figure. The analysis simulated the observed hysteretic response reasonably well. Also, the variation of predicted lateral forces in the bracing unit shows a similar tendency to the test result. The shear cracking in the left and central column and the flexural cracking in the right column were observed in the analysis. Furthermore, the predicted cracking in the retrofit joints were severe, and thus the predicted final failure pattern well corresponded to the test result.

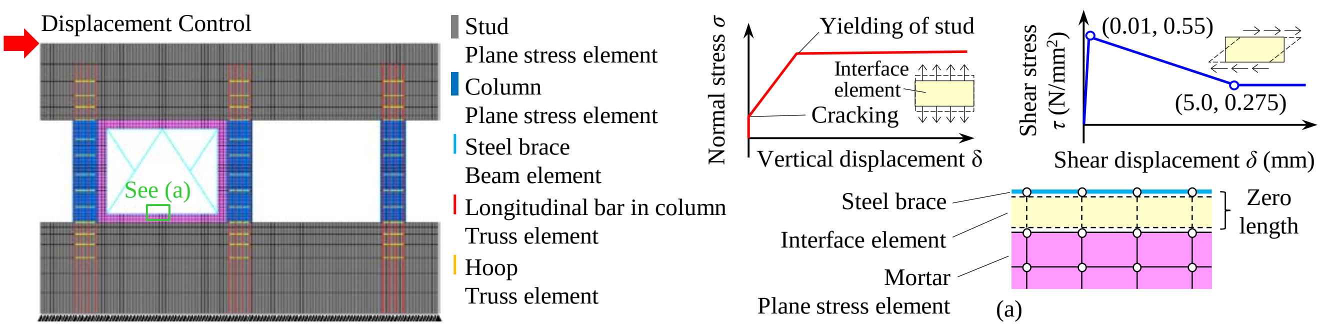

Fig.11 – Mesh division for RCB specimen

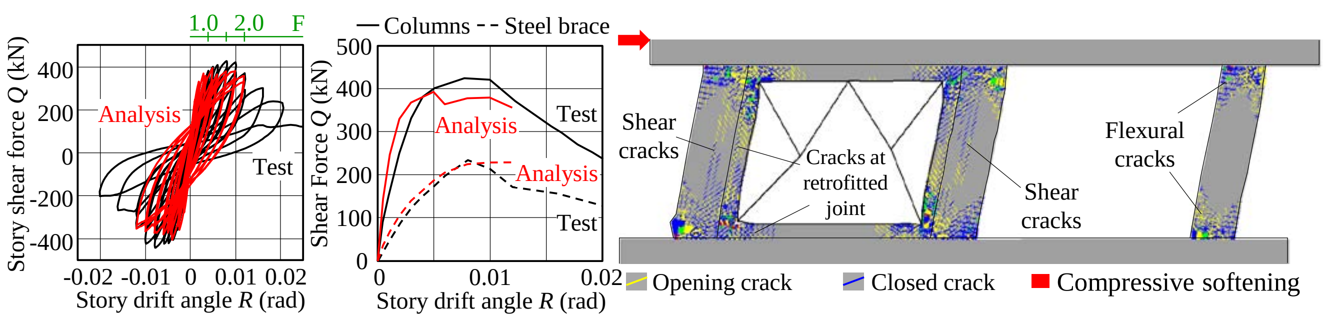

Fig.12 – Analysis results for RCB specimen

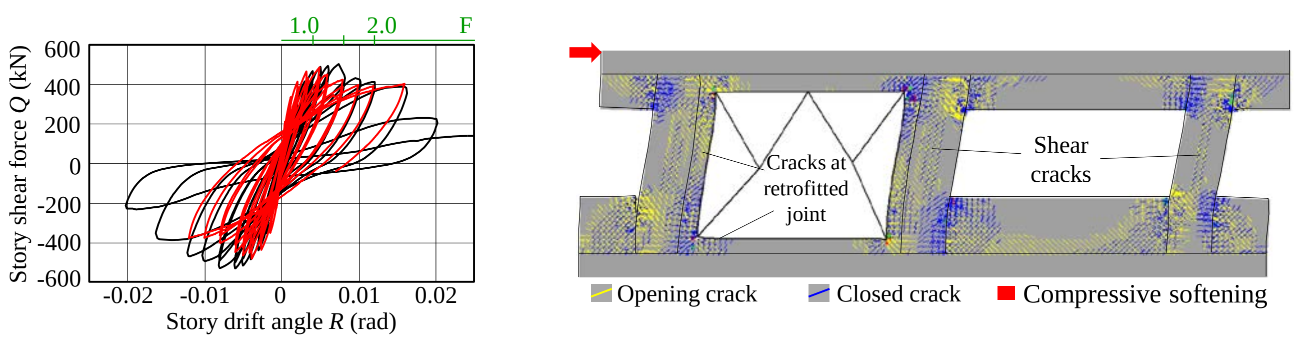

Fig.13 – Analysis results for RCWB specimen

Figure 13 shows the observed and predicted Q - R response and the predicted failure pattern for RCWB. The modeling method and the constitutive law are similar to those of RCW and RCB. As is the case in the previous sections, the analysis with the interface element between the steel frame and the mortar joint was carried out. Although the analysis slightly underestimated the maximum strength under the negative loading, the predicted primary curve and hysteretic behavior simulated the test results satisfactorily. In addition, the shear cracking in all columns was predicted at R = 1/100 rad. by the analysis. The analysis predicted the shear cracking in the columns rather earlier than the test, but the predicted failure pattern well corresponded to the test result.

4.4 Observation on resistant mechanism of each specimen

4.4.1 Redistribution of shear force in R/C columns

Figure 14 shows the normalized resisting shear forces in each member (Q_{member} / Q_{story}) versus the drift angle (R) relations under the positive loading for three specimens; Q_{member} indicates the resisting shear force of each member, and Q_{story} the total story shear force. Note that the shear contribution of the infilled mortar for the retrofitted specimens was added to the shear force of either left or central column with infilled mortar. The resisting shear forces in three columns for RCW were almost equivalent up until R = 1/300. When the drift angle reached R = 4/1000 rad., the ratio of resisting shear force in the central column decreased, but the ratio of resisting shear force in the right column increased. This might be due to the fact that some of the resisting shear force in the central column redistributed to the right column. Even after that, the ratio of resisting shear force in each column changed significantly; thus, suggesting the consecutive redistribution of resisting forces among the columns. In case of two retrofitted specimens, on the other hand, large percentage of the shear force was resisted by the steel braces after R = 2/1000 rad. Furthermore, when the drift angle reached R = 6/1000 rad., 50 percentage of the total story shear force was resisted by the steel braces, and thus the steel bracing unit demonstrated an ability of the retrofitting.

Now, discuss why the failure mode of the right column in RCB, failed in flexure, was different from that in RCWB, failed in shear. The right column of RCB resisted 17 percentage of the total story shear at most, and on the other hand the right column in RCWB resisted 25 percentage of the total story shear force. This suggests an interaction between the ratio of resisting shear force and the failure mode of the column.

4.4.2 Redistribution of axial force in R/C columns and steel braces

Figure 15 shows the normalized resisting axial forces in each member (N_{member} / N_{story}) versus the drift angle (R) relations under the positive loading for three specimens; N_{member} indicates the resisting axial force of each member, and N_{story} the applied total axial force. Note that the axial contribution of the infilled mortar for the retrofitted specimens was added to the axial force of either left or central column with infilled mortar.

First, the constant axial force of N = 540 kN was applied and then the alternative cyclic loading was conducted keeping the axial force constant just like the test. Note that the sum of resisting axial forces in each column becomes always constant. In case of RCW, the normalized resisting axial forces in each column fluctuated significantly just like the resisting shear forces. Now, look at the central column, in which the resisting shear force decreased significantly at R = 4/1000 rad. Since the resisting axial force reduced drastically by the load cycling at the same drift angle, it can be judged that the stability of axial capacity was lost by the shear failure of the column. Furthermore, since the resisting axial force in the right column increased with the reduction of resisting axial force in the central column, the redistribution of resisting axial forces among the columns might be occurred.

In case of two retrofitted specimens, the normalized resisting axial forces fluctuated significantly among the columns just as the resisting shear forces. However, in case of RCB, the normalized resisting axial force in the steel bracing unit changed only slightly, and thus the redistribution of resisting axial forces might be occurred only among three columns. In case of RCWB, on the other hand, the normalized resisting axial force in the steel bracing unit increased due to the significant reduction of resisting axial force in the right column failed in shear.

Again, this suggests the interaction between the ratio of resisting force and the failure mode of the column, and further study on this issue is needed in the future.

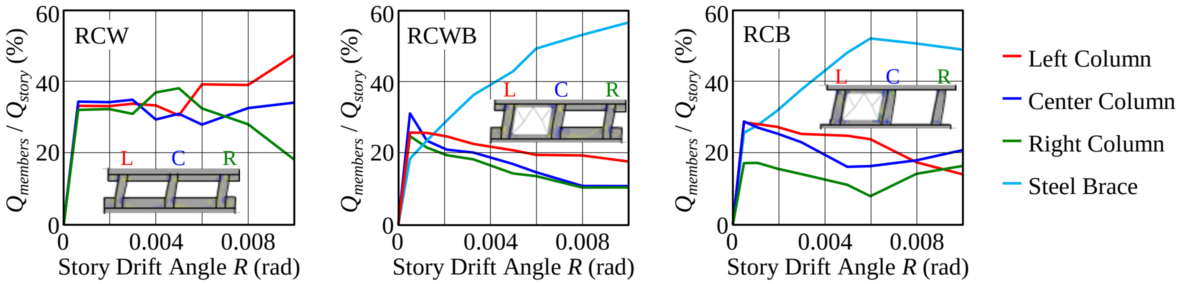

Fig.14 – Redistributions of shear force among three columns and steel brace

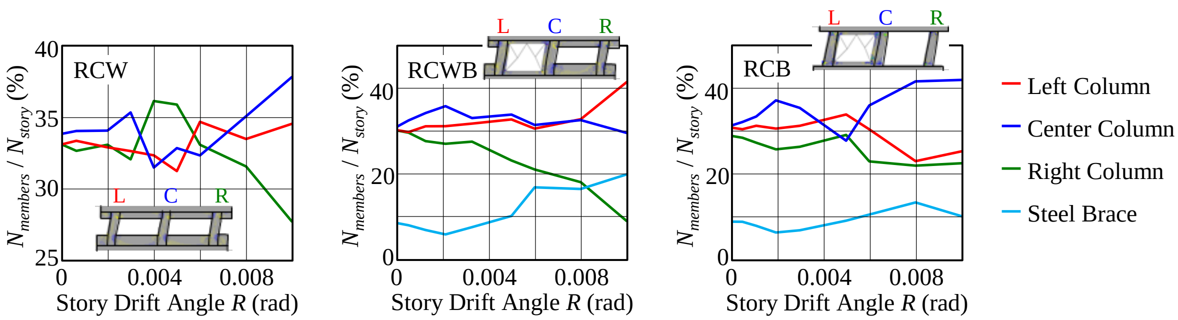

Fig.15 – Redistributions of axial force among three columns and steel brace

6. Conclusions

The following conclusions were derived through the alternative lateral cyclic loading tests on single story and two span R/C sub-frame specimens and the nonlinear finite element analyses:

(1) The RCWB specimen without the structural slit retrofitted with the steel brace unit provided effective performance than the RCB specimen with the structural slits and retrofitted with the steel bracing unit. This may be come from the enhanced deformability by the bond slip behavior of round bars and the fracture of retrofitted joints attributed to the reduced stiffness of columns by the structural slits.

(2) The structural slit is effective for avoiding the shear failure of columns and retaining the axial stability of column.

(3) If the retrofitted joints fracture, the shear transfer mechanism between the steel frame and the R/C skeleton degrades, and then leads to the reduction of resisting shear force in the steel bracing unit.

(4) The FE analysis on RCW, in which included the bond slip behavior of round bars in the columns and the discrete crack model expressed by the interface element between the R/C skeleton and the nonstructural walls, well simulated the test result.

(5) The FE analysis on the retrofitted specimens could simulate the deterioration in the shear transfer mechanism of the steel bracing unit by introducing the interface element in between the steel frame and mortar.

(6) The redistributuion of resisting shear forces and axial forces among the columns and the degradation of axial capacity caused by the shear failure in the columns can be evaluated by the FE analysis.

7. References

[1] Tajima K, Shirai N, Ozaki E, Imai K (2010): FE Modeling and Fiber Modeling for RC Column failing in Shear after Flexural Yielding. *Computational Modelling of Concrete Structures*, *Proceedings of Euro-C 2010*, Rohrmoos/ Schladming, Austria, 737-748.

[2] Naganuma K, Yonezawa K, Kurimoto O, Eto H (2004): Simulation of Nonlinear Dynamic Response of Reinforced Concrete Scaled Model Using Three Dimensional Finite Element Method, *Proceedings of 13th WCEE*, Vancouver, B.C., Canada, Paper No.586.

[3] Nakamura H, Higai T (1999): Compressive Fracture Energy and Fracture Zone Length of Concrete, *Modeling of Inelastic Behavior of RC Structures under Seismic Loads*, ASCE, 471-487.

[4] Takeda T, Yamaguchi T, Naganuma K (1991): An Analytical Model of Reinforced Concrete Panel under In-plane Shear Stress, *Transactions of the 11th international conference on structural mechanics in reactor technology*, **23**(18), 413-418.

[5] Ciampi V, Eligehausen R, Bertero V, Popov P (1982): Analytical Model for Concrete Anchorages of Reinforcing Bars Under Generalized Excitations, *Report No. UCB/EERC-82/23*, University of California, Berkeley.

[6] Matsuoka Y, Nakamura H, Kunieda M, Kawamura S (2011): Evaluation of the Mechanical Behavior of RC Members Using Round Bar by Finite Element Analysis, *Proceedings of the Japan Concrete Institute*, **33**(2), 595-600.

[7] Mishima T, Yamada K, Maekawa, K (1992): Localized Deformational Behavior of a Crack in RC Plates subjected to Reversed Cyclic Loads, *Proceedings of the Japan Society of Civil Engineers*, (442), 161-170. (in Japanese)

[8] Naganuma K (1991): Nonlinear Analytical Model for Reinforced Concrete Panels under In-Plane Stresses : Study on Nonlinear Analytical Method for Reinforced Concrete Wall Structures (Part 1), *Journal of Structural and Construction Engineering*, (421), 39-48. (in Japanese)

[9] The Japan Building Disaster Prevention Association (2001): Seismic Evaluation and Retrofit.

[10] Matsuura M, Kitano A, Goto Y, Joh O (2005): Fundamental Experiments on Bond Characteristics between Concrete and Steel Plates: Influence of Cross-sectional Shapes, Summaries of Technical Papers of Annual Meeting Architectural Institute of Japan. C-1, 1037-1038. (in Japanese)